Adaptive Orthogonal Basis Pursuit for Volumetric Two-Photon Microscopy

Adam S. Charles, Alexander Song, Sue Ann Koay, Jeff L. Gauthier, Stephan Y. Thiberge, David W. Tank and Jonathan W. Pillow
Princeton Neuroscience Institute, Princeton University, Princeton, NJ, 08544

Greedy algorithms have been used extensively in statistical inference and signal processing to provide fast approximate solutions to complex inference problems. One of the most prevalent greedy methods is the Matching Pursuit (MP) family of algorithms (e.g. Orthogonal Matching Pursuit; OMP [1], [2]) for solving sparsity-regularized least-squares optimization programs. Essentially, these methods seek to invert a system of linear equations, i.e. finding a vector $\boldsymbol{x} \in \mathbb{R}^N$ from a vector $\boldsymbol{y} \in \mathbb{R}^M$ such that

$$\boldsymbol{y} = \boldsymbol{A}\boldsymbol{x} + \boldsymbol{\epsilon}, \tag{1}$$

where the columns $\boldsymbol{A}_k \in \mathbb{R}^M$ of the matrix $\boldsymbol{A}$ dictate how the elements of the vector $\boldsymbol{x}$ effect the observation vector $\boldsymbol{y}$, and $\boldsymbol{\epsilon}$ represents the observation noise. MP methods iteratively solve for $\boldsymbol{x}$ by greedily constructing a subset Γ of the columns of $\boldsymbol{A}$ that represent $\boldsymbol{y}$. At each iteration, these methods add the column $\boldsymbol{A}_k$ that has the largest correlation with the residual of the observations after subtracting the contributions from the current representational subset $\boldsymbol{r} = \boldsymbol{y} - \sum_{k\in\Gamma} \boldsymbol{A}_k \boldsymbol{x}_k$. Variants of this basic formula choose the new column(s) to add and construct the residuals in different ways [1], [3], however they all rely on knowing the matrix $\boldsymbol{A}$.

In some applications, precise information about $\boldsymbol{A}$ is not available, however approximate information is known. In such cases, access to multiple measurement vectors $\boldsymbol{y}_t$ for $t = 1 \dots T$ with the same decomposition can compensate for this deficiency. We extend here the MP framework to address cases where the true, unknown $\boldsymbol{A}$ can be approximated by a known $\widetilde{\boldsymbol{A}}$. Ideally, we seek to optimize

$$\left\{\widehat{\boldsymbol{A}}, \widehat{\boldsymbol{X}}\right\} = \arg\min_{\boldsymbol{A},\boldsymbol{X}} \left[\left\| \boldsymbol{Y} - \boldsymbol{A}\boldsymbol{X}^T \right\|_F^2 + \lambda_2 \|\boldsymbol{A} - \widetilde{\boldsymbol{A}}\|_F^2 + \sum_{k=1}^{T} \left(\lambda_1 \|\boldsymbol{x}_k\|_2 + \lambda_{sp} \|\boldsymbol{x}_k\|_1\right) \right], \tag{2}$$

Where $\boldsymbol{Y} = [\boldsymbol{y}_1, \dots, \boldsymbol{y}_T]$, $\boldsymbol{X} = [\boldsymbol{x}_1, \dots, \boldsymbol{x}_T]$. We solve (2) as a greedy OMP algorithm by including an additional shape-projection step adapts the idealized templates to the measurements (addressing the second term in (2)). Denoting $T_\lambda(\cdot)$ as the hard-thresholding operator, and $\mathcal{M}(\cdot)$ as a locality mask (i.e. zeroing out values outside of a certain region), the resulting Sparse Convolutional Iterative Shape Matching (SCISM) algorithm is summarized in Algorithm 1.

The SCISM algorithm was motivated by the application of fluorescence two-photon microscopy (TPM) for calcium imaging [4]. In TPM calcium imaging, neurons are imaged *in-vivo* by introducing fluorescing proteins into the cells that react with the calcium ions associated with neural firing [5]. Typical TPM raster-scans the neural tissue with a diffraction-limited illumination pattern (point-spread function; PSF), resulting in an image representing the illumination at a given time-step along a single 2-D plane of the tissue. To more completely image activity in neural areas in order to better understand the neural processing underlying behavior, neurons outside the plane, in an entire volume, need to be imaged.

Algorithm 1 The SCISM algorithm

Set λ_1, λ_2, λ_{sp}, and K or s_0
Set $m = 1$
Initialize $\boldsymbol{R} = \boldsymbol{Y}$
repeat
  $v_l = \sum_t T_{\lambda_1}\left(\widetilde{\boldsymbol{a}}_l^T \boldsymbol{r}_t\right)^2$
  $k = \arg\max_l v_l$
  $\widehat{\boldsymbol{a}}_k = \frac{1}{N}\sum_t \mathcal{M}\left(\boldsymbol{r}_t\right) \frac{T_{\lambda_2}(\boldsymbol{r}_t^T \widetilde{\boldsymbol{a}}_k)}{\|\mathcal{M}(\boldsymbol{r}_t)\|_2}$
  $\widehat{\boldsymbol{X}} = \arg\min_{\boldsymbol{X}} \left[\|\boldsymbol{Y} - \widehat{\boldsymbol{A}}\boldsymbol{X}\|_F^2 + \lambda_{sp}\sum_k \|\boldsymbol{x}_k\|_1\right]$
  $\boldsymbol{R} = \boldsymbol{Y} - \widehat{\boldsymbol{A}}\widehat{\boldsymbol{X}}$
  $m = m + 1$
until $\min_k \|\boldsymbol{x}_k\|_2^2 \leq s_0$ OR $m >= K$
Output $\widehat{\boldsymbol{A}}, \widehat{\boldsymbol{X}}$

Current methods for volumetric TPM either raster-scan an entire volume, resulting in reduced temporal frame-rates, or extend the PSF in the axial direction (depth) to project entire volumes onto a single image, losing depth information [6], [7]. To preserve depth information, we modify the TPM optics to form two long beams angled in to form a "V"-shaped illumination pattern. Raster-scanning with this illumination pattern creates a 2-D stereoscopic projection of the full volume of neural activity with no loss of temporal resolution (Fig. 1a,b). Once the stereoscopic projections are obtained, isolating pairs of active neural somas allows for the determination of each neuron's 3-D location and activity pattern.

The projection of the somas look approximately like pairs of annuli, and the stereoscopic projection increases the distance between the images linearly with the neuron's depth. If the somas were precisely pairs of annuli, then a dictionary of such shapes could be constructed into a matrix $\boldsymbol{A}$, and each frame in the TPM movie $\boldsymbol{y}_t$ can be decomposed using any number of sparsity-based estimators [8], [9]. In this decomposition, each element of $\boldsymbol{x}_t$ at time t represents the activity of one neuron at a 3D location. Real somas, however, deviate from this ideal shape. We therefore implement SCISM to adapt the idealized shapes to the actual neural shapes.

To test this method, which we term Volumetric Two-photon Imaging of Neurons Using Stereoscopy (vTwINS) [10], we implemented the optical setup and collected data from awake mice situated in a virtual reality (VR) setup. We imaged the mice both in visual cortex V1 and hippocampus area CA1, and the resulting movies were captured neurons at multiple depths. To use SCISM, we set the idealized dictionary $\widetilde{\boldsymbol{A}}$ to images of pairs of annuli at each location, separated by different distances (a total dictionary size of number of pixels $\times$ number of depths). SCISM then iteratively found active neurons, and adapted the located activity profiles to the true soma shapes in the data using the new shape-matching step. The SCISM algorithm was able to extract 3D neural locations and temporal activity for neuron in the imaged tissues (Fig. 1c-f). Both the soma shapes and temporal activity match expected statistics, indicating that vTwINS and SCISM jointly extract volumetric neural activity.

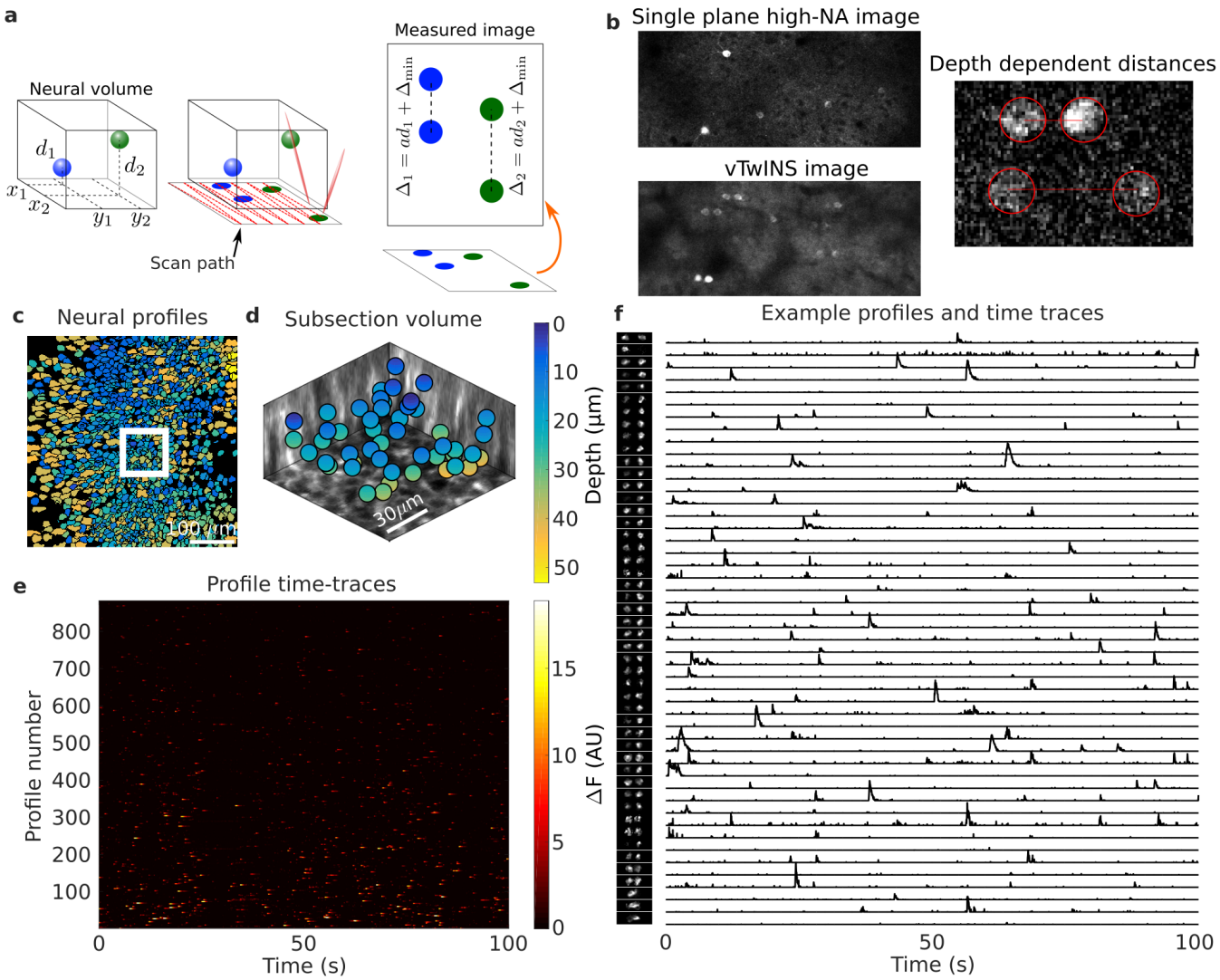

Fig. 1. (a) Depiction of the raster-scan path (red zig-zag pattern) and resulting image of a neural volume using vTwINS. The "V"-shaped PSF (shown here with minimum separation distance of Δ_{min}) results in a measured image where the deeper blue neuron has two nearby images, and the shallower green neuron has more separation between pairs. The separation is affine with depth. (b) Example of a standard TPM image of neural activity, a vTwINS image of the same neural volume, and a subsection depicting neurons at different depths captured with the stereoscopic projection. (c) SCISM run on 25000 frames of data collected from mouse CA1 results in 882 found neurons across the range of depths. Note that the shallow blue in the middle of the field-of-view (FOV) and the deeper orange at the edges captures the curvature of CA1. (d) 3D depiction of neurons found in the subsection of the FOV from (c) shows that neurons at many depths were found. (e) The time traces for the corresponding neural activities represent the expected sparse firing patterns expected, indicating that the activity SCISM captured was actual neural activity. (f) Example pairs of soma images (from the subsection volume in (d))and corresponding time-traces. The deviation in neural shapes from the stereotypical pairs of annuli indicate that SCISM is successful in adapting the idealized shapes to the data.

References

[1] Y. Pati, R. Rezaiifar, and P. Krishnaprasad, "Orthogonal matching pursuit: Recursive function approximation with applications to wavelet decomposition," *Asilomar Conference on Signals, Systems and Computers*, pp. 40–44, 1993.

[2] J. A. Tropp, "Greed is good: Algorithmic results for sparse approximation," *IEEE Transactions on Information theory*, vol. 50, no. 10, pp. 2231–2242, 2004.

[3] D. Needell and J. A. Tropp, "Cosamp: Iterative signal recovery from incomplete and inaccurate samples," *Applied and Computational Harmonic Analysis*, vol. 26, no. 3, pp. 301–321, 2009.

[4] W. Denk, J. H. Strickler, and W. W. Webb, "Two-photon laser scanning fluorescence microscopy," *Science*, vol. 248, no. 4951, pp. 73–6, 1990. [Online]. Available: http://www.ncbi.nlm.nih.gov/pubmed/2321027

[5] M. Mank and O. Griesbeck, "Genetically encoded calcium indicators," *Chem Rev*, vol. 108, no. 5, pp. 1550–64, 2008. [Online]. Available: http://www.ncbi.nlm.nih.gov/pubmed/18447377

[6] R. Lu, W. Sun, Y. Liang, A. Kerlin, J. Bierfeld, J. Seelig, D. E. Wilson, B. Scholl, B. Mohar, M. Tanimoto, M. Koyama, D. Fitzpatrick, M. B. Orger, and N. Ji, "Video-rate volumetric functional imaging of the brain at synaptic resolution," *bioRxiv*, 2016.

[7] W. Yang, J. E. Miller, L. Carrillo-Reid, E. Pnevmatikakis, L. Paninski, R. Yuste, and D. S. Peterka, "Simultaneous multi-plane imaging of neural circuits," *Neuron*, vol. 89, no. 2, pp. 269–84, 2016.

[8] R. Tibshirani, "Regression shrinkage and selection via the lasso," *Journal of the Royal Statistical Society. Series B (Methodological)*, pp. 267–288, 1996.

[9] S. Becker, E. Candes, and M. Grant, "Tfocs: flexible first-order methods for rank minimization," *SIAM Conference on Optimization*, 2011.

[10] A. Song, A. S. Charles, S. A. Koay, J. L. Gauthier, S. Y. Thiberge, J. W. Pillow, and D. W. Tank, "Volumetric two-photon imaging of neurons using stereoscopy (vtwins)," *Nature Methods*, 2017, in press.